O₃ formation sensitivity to precursors and lightning in the tropical troposphere based on airborne observations

Clara M. Nussbaumer[1], Matthias Kohl[1], Andrea Pozzer[1,2], Ivan Tadic[1], Roland Rohloff[1], Daniel Marno[1], Hartwig Harder[1], Helmut Ziereis[3], Andreas Zahn[4], Florian Obersteiner[4], Andreas Hofzumahaus[5], Hendrik Fuchs[5], Christopher Künstler[5], William H. Brune[6], Tom B. Ryerson[7], Jeff Peischl[8,9], Chelsea R. Thompson[8], Ilann Bourgeois[8,9,a], Jos Lelieveld[1,2]and Horst Fischer[1]

[1]Department of Atmospheric Chemistry, Max Planck Institute for Chemistry, 55128 Mainz, Germany
[2]Climate and Atmosphere Research Center, The Cyprus Institute, Nicosia, Cyprus
[3]Deutsches Zentrum für Luft- und Raumfahrt (DLR), Institut für Physik der Atmosphäre, Oberpfaffenhofen, Germany
[4]Institute of Meteorology and Climate Research – Atmospheric Trace Gases and Remote Sensing (IMK-ASF), Karlsruhe Institute of Technology, 76021 Karlsruhe, Germany
[5]Institute of Energy and Climate Research – Troposphere (IEK-8), Forschungszentrum Jülich GmbH, 52428 Jülich, Germany
[6]Department of Meteorology and Atmospheric Science, Pennsylvania State University, University Park, PA 16802, USA
[7]Scientific Aviation, Boulder, CO 80301, USA
[8]National Oceanic and Atmospheric Administration (NOAA) Chemical Sciences Laboratory (CSL), Boulder, CO 80305, USA
[9]Cooperative Institute for Research in Environmental Sciences, University of Colorado Boulder, Boulder, CO 80309, USA
[a]now at: Université Savoie Mont Blanc, INRAE, CARRTEL, 74200 Thonon-les-Bains, France

Key Points:

- $\alpha(CH_3O_2)$ correlated with NO is a powerful metric for indicating O_3 sensitivity and is valid throughout the troposphere.
- O_3 chemistry in the remote tropical lower troposphere is found to be NO_x-sensitive.
- NO emissions from lightning drive O_3 sensitivity in the tropical upper troposphere and induce highly VOC-sensitive chemistry.

Corresponding author: Clara M. Nussbaumer, `clara.nussbaumer@mpic.de`

Abstract

Tropospheric ozone (O_3) is an important greenhouse gas that is also hazardous to human health. O_3 is formed photochemically from nitrogen dioxide (NO_2) (with oxygen and sunlight), which in turn is generated through oxidation of nitric oxide (NO) by peroxy radicals (HO_2 or RO_2). The formation of O_3 can be sensitive to the levels of its precursors NO_x ($\equiv NO + NO_2$) and peroxy radicals, e.g., generated by the oxidation of volatile organic compounds (VOCs). A better understanding of this sensitivity will show how changes in the levels of these trace gases could affect O_3 levels today and in the future, and thus air quality and climate. In this study, we investigate O_3 sensitivity in the tropical troposphere based on in situ observations of NO, HO_2 and O_3 from four research aircraft campaigns between 2015 and 2023, namely, OMO (Oxidation Mechanism Observations), ATom (Atmospheric Tomography Mission), CAFE Africa (Chemistry of the Atmosphere Field Experiment in Africa) and CAFE Brazil, in combination with simulations using the ECHAM5/MESSy2 Atmospheric Chemistry (EMAC) model. We use the metric $\alpha(CH_3O_2)$ together with NO to show that O_3 formation chemistry is generally NO_x-sensitive in the lower and middle tropical troposphere and in a transition regime in the upper troposphere. By distinguishing observations, which are either impacted by lightning or not, we show that NO from lightning is the most important driver of O_3 sensitivity in the tropics. Areas affected by lightning exhibit strongly VOC-sensitive O_3 chemistry, whereas NO_x-sensitive chemistry predominates in regions without lightning impact.

1 Introduction

Ozone (O_3) in the stratosphere is essential to life on this planet through its shielding of the Earth's surface from the sun's shortwave radiation (Staehelin et al., 2001). In contrast, in the troposphere O_3 has adverse effects for plants, human health and the climate (Ainsworth et al., 2012; Nuvolone et al., 2018). O_3 is an important anthropogenic greenhouse gas (besides CO_2 and CH_4) and its impact on global warming is strongest in the upper troposphere where it is most abundant (relative to tropospheric levels), temperatures are coldest and water vapor, which acts as a natural greenhouse gas, is sparse (Cooper et al., 2014; Iglesias-Suarez et al., 2018; IPCC, 2023). This influence of O_3 on the radiative budget is particularly pronounced in tropical latitudes (30°S to 30°N) (Lacis et al., 1990; Iglesias-Suarez et al., 2018; Skeie et al., 2020). O_3 is additionally an important precursor for OH radicals, which in turn control the atmospheric oxidizing capacity (Lelieveld et al., 2016).

Ozone in the troposphere can originate from transport processes from the stratosphere and photochemical formation. While the exact source distribution has not yet been fully understood up to this point, it is almost certain that photochemical production is the dominant source of O_3 in the troposphere (Lelieveld & Dentener, 2000; Cooper et al., 2014; Archibald et al., 2020). Nitrogen oxides ($NO_x \equiv NO + NO_2$) and volatile organic compounds (VOCs) are photochemical precursors for O_3 in the troposphere. NO_x is mostly emitted in the form of NO and converted to NO_2 in the presence of peroxy radicals (mostly HO_2 and CH_3O_2), shown in Reactions (R1) and (R2). Peroxy radicals in turn are formed through oxidation of VOCs or carbon monoxide (CO) by OH radicals (Crutzen, 1988; Pusede et al., 2015; Nussbaumer & Cohen, 2020).

$$NO + HO_2 \longrightarrow NO_2 + OH \tag{R1}$$

$$NO + RO_2 \longrightarrow NO_2 + RO \tag{R2}$$

NO_2 forms O_3 in the presence of sunlight and oxygen from the air via Reaction (R3).

$$NO_2 + O_2 \xrightarrow{h\nu} NO + O_3 \tag{R3}$$

Precursor sources at the surface are combustion processes (vehicle engines, vessels, industrial activities, etc.), biomass burning and soil emissions for NO and mostly evaporative emissions, including volatile chemical products (personal care products, detergents, etc.), as well as biogenic emissions from vegetated areas for VOCs (Pusede et al., 2015; McDonald et al., 2018). Aircraft and lightning are sources of NO at higher altitudes in the troposphere.

Depending on the precursor concentrations, O_3 formation can be sensitive to either NO_x or VOCs, the latter represented by peroxy radicals. A detailed analysis and discussion of our current understanding of O_3 sensitivity can be found in Nussbaumer et al. (2023). Briefly, for low NO_x, referred to as NO_x-sensitive O_3 chemistry, VOCs and therefore peroxy radicals are present in excess. Peroxy radicals undergo Reactions (R1) and (R2) with NO and further react with themselves in radical recombination reactions or undergo auto oxidation. O_3 formation generally increases with increasing NO. O_3 chemistry is VOC-sensitive when NO_x is available in excess. A maximum level of ozone production is reached when the available peroxy radicals react with NO to form NO_2. The impact of increases in NO_x on O_3 concentrations for VOC-sensitive O_3 chemistry changes with the altitude, which we hypothesize is due to the fraction of NO_2. At the surface, O_3 formation decreases with increasing NO_x due to the reaction of OH radicals with NO_2 (instead of VOCs to generate peroxy radicals), which becomes relevant when NO_x is more abundant than reactive VOCs. Observations of decreasing O_3 at high NO_x are often reported in literature, for example, Nussbaumer and Cohen (2020), Sicard et al. (2020) or Gough and Anderson (2022). In the upper troposphere, the reaction of NO_2 with OH only plays a minor role - likely because daytime NO_2 is sparse as the NO_x equilibrium is shifted towards NO. Consequently, O_3 is much less responsive to NO changes. We have shown this effect of O_3 in the upper troposphere in Nussbaumer et al. (2023).

In order to understand and predict the response of O_3 towards changes in NO_x and VOCs, it is essential to investigate which precursor O_3 is sensitive to, given its importance for air quality and climate. Various metrics exist to determine which sensitivity prevails, including the response of ozone production $P(O_3)$ to changes in NO_x, the weekend effect or the HCHO to NO_2 ratio. A detailed review and comparison of the most common metrics in the literature is presented in Liu and Shi (2021) for the surface and Nussbaumer et al. (2023) for the global troposphere. We found that most of these metrics are only applicable at the surface, but not in the upper troposphere. Briefly, mixing ratios of trace gases vary significantly throughout the troposphere and definitions for the surface, for example, $P(O_3)$ changes with NO_x or a specific threshold for the HCHO to NO_2 ratio do not apply at high altitudes. A detailed discussion can be found in Nussbaumer et al. (2023). Instead, we have developed a new metric, $\alpha(CH_3O_2)$, to determine O_3 sensitivity, which is valid throughout the entire troposphere (Nussbaumer, Crowley, et al., 2021; Nussbaumer et al., 2022). $\alpha(CH_3O_2)$ presents the ratio of methyl peroxy radicals CH_3O_2 (a proxy for VOCs) which react with NO and promote O_3 formation in competition with the peroxy radical self-reaction which inhibits O_3 formation. We present more details including the calculation of $\alpha(CH_3O_2)$ in Section 2.1.

$\alpha(CH_3O_2)$ was originally proposed as an indicator for formaldehyde formation and applied to three stationary ground-site measurements across Europe in Cyprus, Germany and Finland (Nussbaumer, Crowley, et al., 2021). $\alpha(CH_3O_2)$ identified NO_x-sensitive O_3 chemistry in southeastern Europe and VOC-sensitive O_3 chemistry in central Europe, which is in line with results obtained via the HCHO to NO_2 ratio, a metric dating back to studies by Sillman (1995). In Nussbaumer et al. (2022), we used $\alpha(CH_3O_2)$ to indicate a change in upper tropospheric O_3 sensitivity in response to reduced air traffic (and a 55% reduction in NO_x mixing ratios) during the COVID-19 lockdowns over Europe,

which common metrics would have failed to identify. We have recently investigated O_3 sensitivity in the upper tropical troposphere based on modeling simulations by a general circulation model and found lightning as the most important driver of VOC-sensitive O_3 chemistry (Nussbaumer et al., 2023). Generally, these studies have underlined that NO_x is most relevant in O_3 formation and sensitivity and that the abundance of VOCs only plays a subordinate role.

There are numerous studies that have investigated O_3 sensitivity to NO_x and VOC levels at the surface and they almost exclusively focus on urban areas (Li et al., 2019; Jaffe et al., 2022; Zhao et al., 2022; Akimoto & Tanimoto, 2022). While this is highly relevant with respect to air quality and human health, it is also important to investigate more remote locations particularly in regard to future emission changes. For example, with increasing temperatures and decreasing precipitation one could expect to see increases in biomass burning, resulting in emission of NO_x in the remote rainforest (Bray et al., 2021). In combination with the high levels of VOCs in these areas, O_3 could increase drastically locally, and in turn harm the natural vegetation and agricultural crops (Ainsworth et al., 2012; Pope et al., 2020). At the same time, ongoing industrialization in the Global South will likely impact ozone concentrations in the tropical troposphere (Gaudel et al., 2024). In contrast to surface-based analyzes, research on O_3 sensitivity in the upper troposphere is scant and has not been investigated in detail since the studies of Brasseur et al. (1996), Jaeglé et al. (1998), Wennberg et al. (1998) and Jaeglé et al. (1999) around 25 years ago, who concluded that O_3 chemistry was NO_x-sensitive in the upper troposphere over the United States based on box-model simulations. Of note, the observations for high NO_x did not match the model predictions in Jaeglé et al. (1998) and Jaeglé et al. (1999). We suggest that O_3 production is an unsuitable metric for indicating O_3 sensitivity at high altitudes. This could be (partly) due to the terminating reaction $OH + NO_2$ (forming HNO_3), which does not seem to play a significant role for low NO_2 mixing ratios in the upper troposphere.
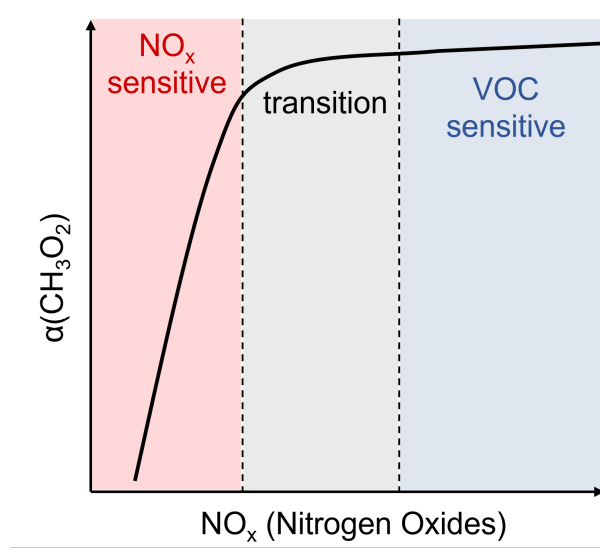
This study investigates O_3 chemistry in the tropical troposphere based on airborne observations during four aircraft campaigns, namely OMO, ATom, CAFE Africa and CAFE Brazil, between 2015 and 2023. We compare in situ observations with modeled data by the ECHAM5/MESSy2 Atmospheric Chemistry (EMAC) model and we investigate the differences in trace gas concentrations and vertical profiles between the individual campaigns (and regions). We use $\alpha(CH_3O_2)$ to identify O_3 sensitivity towards its precursors in the tropical troposphere, with a particular focus on the role of lightning.

While we have previously analyzed O_3 chemistry in the upper tropical troposphere based on model simulations (Nussbaumer et al., 2023), this is the first study to investigate the question of O_3 sensitivity at these altitudes based on in situ observations using the metric $\alpha(CH_3O_2)$. To our knowledge, $\alpha(CH_3O_2)$ is currently the only available metric reliably indicating which precursor O_3 is sensitive to at altitudes at which common tools fail and the impact of O_3 as a greenhouse gas is strongest.

2 Observation and Methods

2.1 O_3 Sensitivity Metric $\alpha(CH_3O_2)$

$\alpha(CH_3O_2)$ was originally developed for identifying HCHO (formaldehyde) production pathways. It presents the share of CH_3O_2 (methyl peroxy radicals) reacting with NO or OH radicals forming HCHO versus the peroxy self-reaction ($CH_3O_2 + HO_2$) forming CH_3OOH (Nussbaumer, Crowley, et al., 2021). The reaction of CH_3O_2 with NO also yields NO_2, which forms O_3 via Reaction (R3), while the reaction of CH_3O_2 with HO_2 represents a termination reaction of the O_3 formation process (which is relevant for a low-NO_x environment). The reaction of CH_3O_2 with OH contributes to HCHO, but not to O_3 formation, and generally only plays a minor role compared to the pathway via NO

Figure 1. Identifying the dominant O_3 sensitivity using $\alpha(CH_3O_2)$ (adapted from Nussbaumer, 2023).
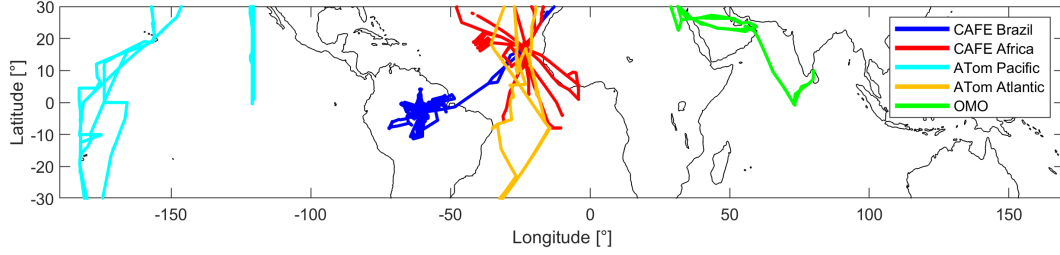
and HO_2. Therefore, it can be disregarded when studying O_3 sensitivity. Hence, $\alpha(CH_3O_2)$ is calculated via Equation (2). We only use positive values for determining $\alpha(CH_3O_2)$ to ensure that the resulting value is between 0 and 1.

$$\alpha(CH_3O_2) = \frac{k_{CH_3O_2+NO} \times [NO]}{k_{CH_3O_2+NO} \times [NO] + k_{CH_3O_2+HO_2} \times [HO_2]} \tag{2}$$

A detailed description of $\alpha(CH_3O_2)$ can be found in Nussbaumer, Crowley, et al. (2021), Nussbaumer et al. (2022) and Nussbaumer et al. (2023). Briefly, for low NO_x concentrations, CH_3O_2 react with both NO and HO_2 and increases in NO lead to increases in $\alpha(CH_3O_2)$. O_3 chemistry is NO_x-sensitive. For high NO_x concentrations, most available CH_3O_2 reacts with NO and changes in NO have no impact on $\alpha(CH_3O_2)$, as O_3 sensitivity is limited by the availability of peroxy radicals (which represent the abundance of VOCs). Figure 1 schematically shows how to use $\alpha(CH_3O_2)$ to identify prevailing O_3 sensitivity (Nussbaumer, 2023). O_3 concentrations increase with increasing NO_x when O_3 chemistry is NO_x-sensitive. For VOC-sensitive O_3 chemistry at the surface, O_3 formation decreases with increasing NO_x due to the reaction of OH and NO_2. In the upper troposphere, O_3 concentrations reach a maximum and remain unresponsive to changes in NO_x.

2.2 Aircraft Campaigns

Figure 2 presents an overview of the flight tracks of the four research aircraft campaigns discussed in this paper. These are OMO (Oxidation Mechanism Observations), ATom (Atmospheric Tomography Mission), CAFE Africa (Chemistry of the Atmosphere Field Experiment in Africa) and CAFE Brazil. The ATom campaign was divided into measurements over the Atlantic and the Pacific Ocean. Detailed information on the individual campaigns and the respective measurements are provided in the following subsections. We filtered all data for the tropical latitudes between 30°S and 30°N and for the troposphere with a threshold of 100 ppbv for O_3. We use a 1-minute average of the measurements, brought to the NO timestamp, for this analysis.

Figure 2. Overview of the flight tracks (filtered by tropical latitudes between 30°S and 30°N) for the four aircraft campaigns OMO (green), ATom, CAFE Africa (red) and CAFE Brazil (blue). The ATom campaign was separated into data over the Atlantic (orange) and the Pacific Ocean (cyan).

2.2.1 OMO 2015

The aircraft campaign OMO (Oxidation Mechanism Observations) took place in July and August 2015 over the Indian Ocean and the Middle East using the HALO (High Altitude LOng range) research aircraft. The campaign comprised 17 research flights (some on the same day) with campaign bases in Paphos in Cyprus (34.72°N, 32.49°E) and Gan in the Maldives (0.69°S, 73.16°E). More details can be found in Lelieveld et al. (2018) and Tomsche et al. (2019). Nitric oxide was measured via chemiluminescence with the two-channel AENEAS (Atmospheric nitrogen oxides measuring system) instrument with a detection limit of 7 pptv and a measurement uncertainty of 8 % (for 0.5 ppbv) (Ziereis et al., 2000; Stratmann et al., 2016). HO_2 was measured via laser-induced fluorescence with the HORUS (Hydroxyl Radical Measurement Unit based on fluorescence Spectroscopy) and the AirLIF instruments (Novelli et al., 2014; Marno et al., 2020; Künstler, 2020). The HORUS instrument has a detection limit of 1.2 pptv for HO_2 at the surface and 0.23 pptv above 14 km. The accuracy is typically between 20 % and 40 %. The detection limit and uncertainty for the Air-LIF instrument are also altitude-dependent. The detection limit (signal-to-noise ratio = 2, 40 s time resolution) is generally less than 1 pptv and about 0.1 pptv above 5 km. The data accuracy is between 15 and 35 %. Neither of the HO_2 measurements was continuous over the entire campaign. The data from the five overlapping flights showed good agreement and we therefore combined the data from the two instruments (research flights 1-6 (21.07.-06.08.2015) from AirLIF and 7-17 (08.08.-27.08.2015) from HORUS) to obtain a full dataset. Ozone was measured with the FAIRO (Fast AIRborne Ozone) instrument using a dry chemiluminescence detector, calibrated by a 2-channel UV photometer, with an uncertainty (10 Hz) of 2.5 % or 2 ppbv (Zahn et al., 2012; Obersteiner, 2023).

2.2.2 ATom 2016-2018

The aircraft campaign ATom (Atmospheric Tomography Mission) consisted of four deployments between 2016 and 2018 in summer 2016, winter 2017, fall 2017 and spring 2018 with the NASA DC-8 aircraft, operated by the NASA Armstrong (Dryden) Flight Research Center. A total of 47 scientific flights were carried out over the almost 2-year period. Each deployment circumnavigated the globe once. More details on the campaign, including all flight tracks, can be found in Thompson et al. (2022) and via the campaign website (NASA, 2022). For this study, we used the data measured in the tropical regions between 30°S and 30°N latitude and additionally separated them into two geographic regions over the Pacific and the Atlantic Ocean (see Figure 2 in cyan and orange, respectively). NO and O_3 were measured via chemiluminescence using an O_3-induced and a NO-induced technique, respectively. The measurement uncertainties (1 Hz data) were

5 % for NO and 2 % for O_3, with a precision of 6 pptv and 15 pptv, respectively (Bourgeois et al., 2021, 2022). HO_2 was measured via laser-induced fluorescence with a 2σ accuracy of 35 %. Details can be found in Faloona et al. (2004).
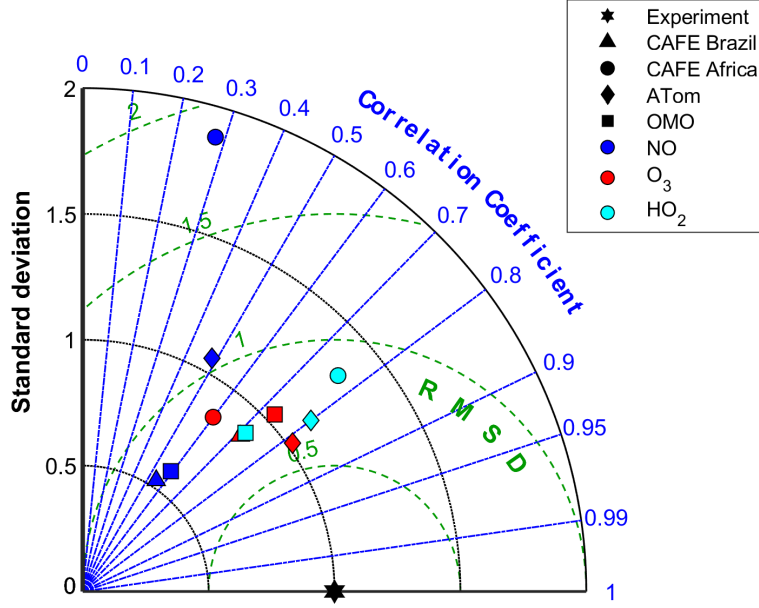
2.2.3 CAFE Africa 2018

The Chemistry of the Atmosphere Field Experiment in Africa (CAFE Africa) took place in August and September 2018 from Sal on Cabo Verde (16.75°N, 22.95°W). Fourteen scientific flights were performed with the HALO research aircraft, mostly over the Atlantic Ocean. Details on the campaign and measurements can be found in Tadic et al. (2021). Nitric oxide was measured with the chemiluminescence instrument (CLD 790 SR, ECO Physics, Dürnten, Switzerland) NOAH (Nitrogen Oxides Analyzer for HALO) with a detection limit of 5 pptv (1 min) and an uncertainty of 6 %. The instrument is described in detail in Tadic et al. (2020) and Nussbaumer, Parchatka, et al. (2021). Ozone was measured with the FAIRO instrument, as described in Section 2.2.1. HO_2 was measured with the HORUS instrument and has an uncertainty of approximately 50 %. Due to the difficulty in determining an experimental calibration factor for the HO_2 data set, a value of 2.5 was estimated based on comparison with the EMAC model and its performance in measuring hydrogen peroxide (H_2O_2) (Hamryszczak et al., 2023).

2.2.4 CAFE Brazil 2022-2023

The Chemistry of the Atmosphere Field Experiment in Brazil (CAFE Brazil) took place in December 2022 and January 2023 with the HALO research aircraft from Manaus in Brazil (3.03°S, 60.04°W). Twenty scientific flights (including four transfer flights from Oberpfaffenhofen, Germany with a stopover in Sal, Cabo Verde) were carried out over a two-month period over the pristine rain forest as well as deforested regions and urbanized areas. The scientific goals of the campaign included the investigation of photochemical processes impacted by high VOC/low NO_x environments, convective events throughout the troposphere and particle formation. The campaign was timed to occur at the seasonal transition which enabled capture of measurements during the dry season in December and the rainy season in January. Nitric oxide was measured with the NOAH instrument with a detection limit of 6 pptv (1 min) and an uncertainty of 5 %. O_3 data were obtained with the FAIRO instrument with a data uncertainty of 2.5 % or 2 ppbv. Final data for HO_2 measurements are not available at this point and we therefore include modeled data from EMAC simulations, as described in Section 2.3 in our analysis.

2.3 Modeling

Modeled data for NO, O_3, HO_2, temperature and pressure were obtained with the EMAC model. The ECHAM/MESSy Atmospheric Chemistry (EMAC) model is a numerical chemistry and climate simulation system that includes sub-models describing tropospheric and middle atmosphere processes and their interaction with oceans, land and human influences (Jöckel et al., 2016). It uses the second version of the Modular Earth Submodel System (MESSy2) to link multi-institutional computer codes. The core atmospheric model is the 5th generation European Centre Hamburg general circulation model (Roeckner et al., 2006, ECHAM5). The physics subroutines of the original ECHAM code have been modularized and reimplemented as MESSy submodels and have continuously been further developed. Only the spectral transform core, the flux-form semi-Lagrangian large scale advection scheme, and the nudging routines for Newtonian relaxation are remaining from ECHAM. Here we use different numerical results from different integrations and with different set-up, mostly presented in previous publications. Description of the set-up of the EMAC model for CAFE Africa, OMO and ATom campaigns can be found in Tadic et al. (2021), Lelieveld et al. (2018) and Nussbaumer et al. (2022), respec-

Figure 3. Overview of the model performance, presented in a Taylor diagram (Taylor, 2001). Triangles represent modeled data for the CAFE Brazil campaign, circles the CAFE Africa campaign, diamonds the ATom campaign and squares show modeled data for the OMO campaign. Blue colors represent NO, red shows O_3 and HO_2 data is cyan.

tively. The simulation for the CAFE Brazil measurement campaign was performed at a spectral horizontal resolution of T63, equivalent to approximately 180 x 180 km at the equator, with 90 vertical levels up to an altitude of 0.1 hPa. Weak "nudging" was applied, guiding the simulation towards meteorological reanalysis data (ERA5, Hersbach et al., 2020) from the European Centre for Medium-Range weather forecasts (ECMWF). Global anthropogenic emissions of reactive gases and aerosols at the surface were obtained from the Community Emission Data System (CEDS, McDuffie et al., 2020) and aircraft emission data were taken from the CAMS Global aviation emissions (CAMS-GLOB-AIR; Granier et al., 2019), both for the year 2019. Updated emission inventories tailored to the campaign timeframe were not available yet. Additionally, NO_x emissions from lightning were integrated into the simulation using the parameterization proposed by Grewe et al. (2001), scaled to 2.6 Tg (N) per year. This value falls within the lower end of the estimate of 2–8 Tg (N) per year provided by Schumann and Huntrieser (2007), yields consistent tropospheric O_3 and demonstrates the best agreement with observations. While this study is based on in situ observations, we include the modeled data for a comparison to identify how well the data sets align. Additionally, we use HO_2 modeled data for CAFE Brazil as final experimental data are not available at this point.

3 Results

3.1 Model Performance

Figure 3 shows a normalized Taylor diagram presenting the model performance for each campaign and trace gas investigated in this analysis (Taylor, 2001). The experimental data is represented by the black hexagram, with a normalized standard deviation of 1, a correlation coefficient of 1 and root-mean-square difference of 0. The closer the colored data points, representing the model data sets, are located to the experimental reference value, the better the model performance. For most of the modeled data sets, stan-
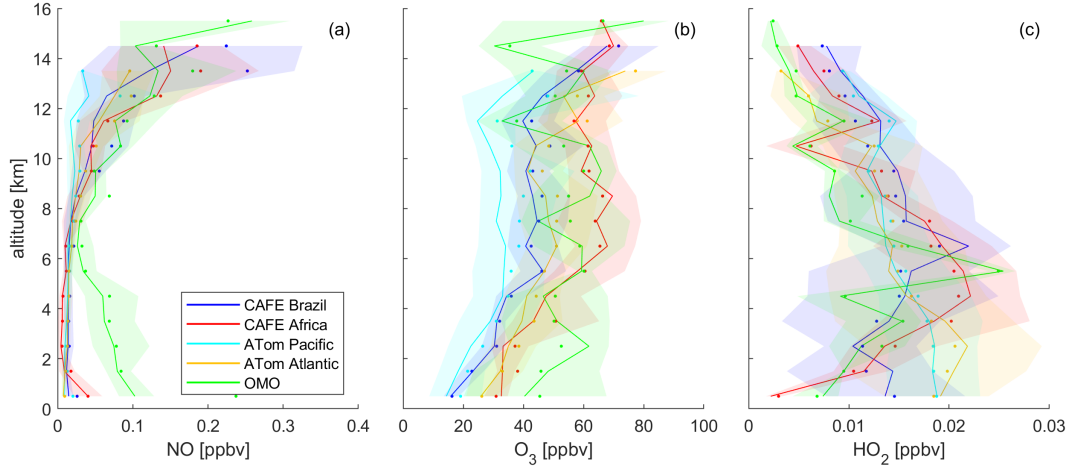
dard deviations are similar to those from their experimental counterparts. Deviations are observed for NO (blue): CAFE Brazil (triangles) and OMO data sets (squares) have lower standard deviations by a factor of 2 and the CAFE Africa data set (circles) has a larger standard deviation (almost twice as large). The latter additionally shows only an intermediate correlation coefficient of around 0.3. All other modeled data sets show a good correlation with the experiment with a correlation coefficient of 0.5 or larger. The ATom data set (diamonds) for O_3 even reaches values of > 0.8. The O_3 (red) and HO_2 data sets (cyan) for the different campaigns show a similar model performance, whereas differences could be seen between the quality of the different NO data sets. This could be due to the difficulty in accurately representing lightning in the model. A further comparison between modeled and measured data can be found in Figures S1–S5 of the Supporting Information, where we show the vertical profiles of each trace gas. Tables S1–S5 show an overview of the number of data points per altitude bin used to create the vertical profiles. The model may have difficulties representing the intermittent nature of convection and lightning, illustrated by the larger spread in the upper troposphere (UT). HO_2 modeled and experimental vertical profiles align well for OMO, CAFE Africa and ATom and the Taylor diagram also shows a good model performance, which verifies the use of the modeled HO_2 data set for CAFE Brazil.

3.2 Vertical Distribution

Figure 4 presents the vertical profiles of (a) NO, (b) O_3 and (c) HO_2 measured during the investigated campaigns. During CAFE Brazil, CAFE Africa and ATom over the Pacific and the Atlantic Ocean, NO was low in the lower and middle troposphere with median values below 20 pptv up to 8 km altitude. The values during the OMO campaign were much larger up to 5-6 km; however, only around 5 % of all data points were measured at these low altitudes and they were exclusively located in proximity to airports. Therefore, it can be assumed that the large NO mixing ratios represent localized airport emissions. At high altitudes, the profiles show elevated mixing ratios. Above 10 km, NO median values were overall highest during CAFE Africa with 118 pptv, followed by OMO with 108 pptv and CAFE Brazil with 61 pptv. These campaigns were also characterized by large maximum values for NO, sometimes above 2 ppbv, which indicates strong lightning activity. Median and peak values were generally lower during the ATom campaign with mixing ratios of 51 pptv and 0.43 ppbv, respectively, over the Atlantic and only 20 pptv and 0.48 ppbv, respectively, over the Pacific Ocean. These observations underline the impact of lightning at these altitudes and latitudes. We have determined a filter for lightning activity which defines data points above 2 km with NO mixing ratios above 100 pptv as impacted by lightning. This includes both fresh and aged lightning emissions. For OMO, this identifies approximately 50 % of the data points as being impacted by lightning, followed by CAFE Africa with around 40 % and CAFE Brazil with approximately 20 %. For ATom, only few data points were impacted by lightning with below 10 % over the Atlantic Ocean and less than 5 % over the Pacific Ocean, the latter explaining the almost unchanging (with altitude) cyan vertical profile.

These observations demonstrate two important features impacting lightning, which are the time of year and the distance from tropical landmasses. The maximum of deep convection, which is associated with lightning activity and large NO emissions, changes its location throughout the year due to seasonal, meridional changes in convective activity. While over the year as a whole, this maximum is located close to the equator ($\pm 5\,°$), in January, it is mostly found in the Southern Hemisphere and in July in the Northern Hemisphere (compare Figure I2 in Yan (2005)). The region of maximum deep convection is also referred to as the ITCZ (Inter Tropical Convergence Zone). CAFE Africa and OMO were carried out in August/September mostly coinciding with the location of the ITCZ, explaining high lightning intensity. CAFE Brazil took place in December and January and the flight track latitudes tended to be slightly northward, but still close to the location of the ITCZ at that time of the year, which could be a potential explanation

Figure 4. Vertical profiles of (a) NO, (b) O_3 and (c) HO_2 for tropical latitudes for the investigated aircraft campaigns. Lines and shades represent the median values and the 25th/75th percentiles, respectively. Dots show the mean values in the center of each 1 km altitude bin.

for fewer data points with identified lightning impact. The impact of the time of year can be neglected for the ATom campaign as the vertical profiles present medians and averages across all four deployments. Lightning was lowest over the remote Pacific Ocean during ATom, in line with our understanding of lightning formation, which is thought to require solid particles for the formation of light ice particles. In fact, solid particles, such as dust or sand, are usually more abundant over or in proximity to land masses, which makes lighting strongest over the (tropical) continents (Christian et al., 2003; Verma et al., 2021; Nussbaumer, Tadic, et al., 2021). Likewise, low lightning activity was observed over the Atlantic Ocean during ATom. The NO observations for CAFE Africa were much larger in comparison to the ATom Atlantic data in the upper troposphere, although the two data sets are derived from neighboring geographical areas. The location of the ITCZ throughout the year cannot explain the difference, as the median NO mixing ratios measured during the ATom deployment in August were similar to the one in February. However, the ATom Atlantic data set shrinks when filtering the tropical latitudes for different times of the year, whereas CAFE Africa ran many flights in the same region and therefore provides an improved representation of the region. Additional differences may arise from meteorological conditions or differences in wildfire activity between years (ATom Atlantic in August 2016 and CAFE Africa in August 2018).
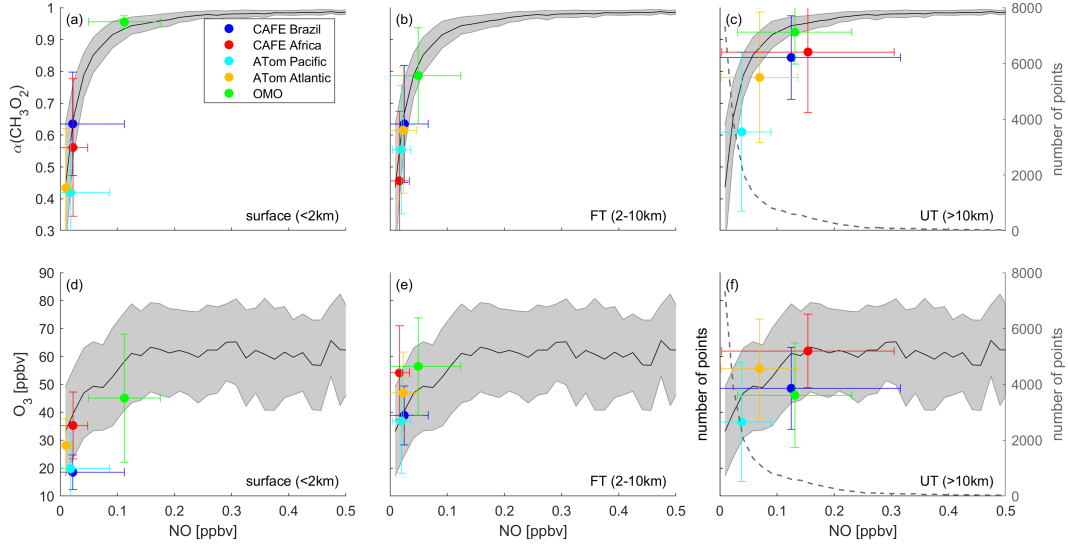
Figure 4 (b) presents the vertical profiles of O_3. Generally, O_3 increased with altitude and increasing proximity to the stratosphere, where O_3 is abundant. The lowest mixing ratios were observed during ATom over the Pacific Ocean with median values below 15 ppbv at the surface and 28 ppbv above 10 km. This correlates well with low NO mixing ratios throughout the tropospheric column, which when oxidized to NO_2 is the photochemical source of tropospheric O_3. The low mixing ratio between 11 and 12 km altitude could indicate convective updraft from the O_3-poor marine boundary layer. CAFE Brazil O_3 mixing ratios were similar to those observed during ATom Pacific up to 5 km altitude. Above this altitude, O_3 median values during CAFE Brazil were approximately 10 to 15 ppbv higher. The vertical profile also shows the typical S-shape observed for convective updraft to the upper troposphere. The ATom Atlantic O_3 vertical profile shows a similar shape to the one observed during CAFE Brazil with median mixing ratios of 26 ppbv at the surface and 52 ppbv above 10 km. The vertical O_3 profile for OMO does not show a particular trend with altitude, but a quite strong fluctuation with median values between 30 and 80 ppbv is evident. O_3 mixing ratios during CAFE Africa were

around 30 ppbv (median) at the surface and increased strongly up to 60–70 ppbv at 7 km, above which they remained mostly unaffected by altitude. The large difference of around 20 ppbv between O_3 mixing ratios for CAFE Africa and ATom Atlantic in the free troposphere could have likely arisen from the time of year as the profiles align well when only considering August data from the ATom campaign. This could be due to wildfire emissions in the Southern Hemisphere at that time of year.

Figure 4 (c) presents the vertical profiles of HO_2. Mixing ratios were mostly low and comparable to upper tropospheric values at the surface and showed a maximum in the free troposphere between 3 and 7 km altitude. Quite large differences between the campaigns can be observed at the surface with median values ranging from around 2 pptv for CAFE Africa and approximately 20 pptv for ATom. However, the uncertainties of the HO_2 measurements were usually highest at low altitudes and the profiles mostly show large and overlapping error shades (representing the 25th and 75th percentiles). In the upper troposphere, HO_2 measured during OMO and ATom Atlantic was lowest with a median of 4 pptv above 12 km, followed by CAFE Africa with 7 pptv and CAFE Brazil and ATom Pacific with 10-11 pptv.
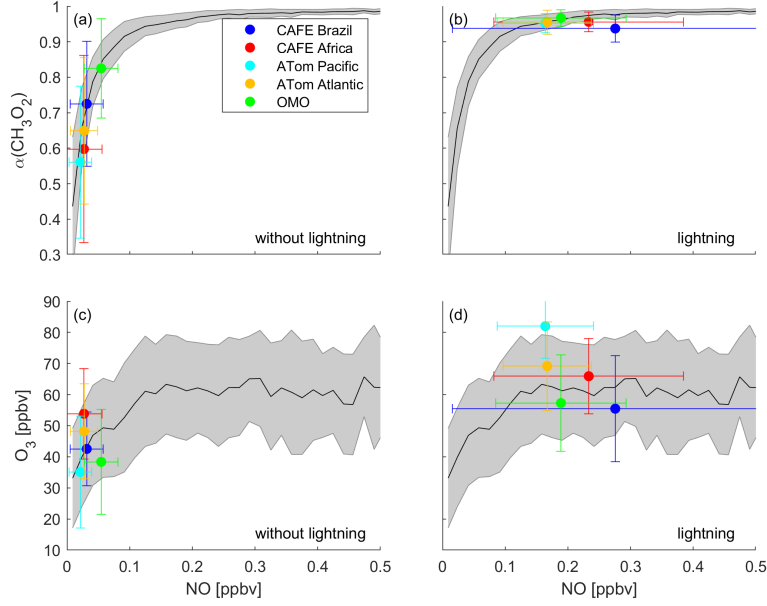
3.3 O_3 Sensitivity

As described above, $\alpha(CH_3O_2)$ can be used to determine O_3 sensitivity to its precursors. $\alpha(CH_3O_2)$ is plotted in Figure 5 (a)-(c) for all campaigns. The black line shows the average $\alpha(CH_3O_2)$ binned to NO mixing ratios for all available data points and therefore presents the tropical "background". The individual curves for each campaign do not show significant differences. As expected, $\alpha(CH_3O_2)$ increases strongly with NO for low ambient NO mixing ratios, which demonstrates NO_x-sensitive O_3 chemistry. For an increase in NO from 1 to 10 pptv, $\alpha(CH_3O_2)$ increases by almost 0.5. For higher NO, $\alpha(CH_3O_2)$ becomes unresponsive to changes in NO, which is characteristic of VOC-sensitive O_3 chemistry. For an NO increase from 10 to 50 pptv, $\alpha(CH_3O_2)$ shows an increase of less than 0.1. Panel (c) additionally shows the number of data points in each NO bin by the gray dashed line. The vast majority of the data points is characterized by NO mixing ratios below 0.1 ppbv. The number decreases to a few dozen data points for the high-NO bins. The colored data points represent the campaign averages and the three panels of each row show different altitudes. Figure 5 (a) presents the averages below 2 km altitude. CAFE Brazil, CAFE Africa, ATom Pacific and ATom Atlantic showed a clear NO_x-sensitive chemistry at the surface, as the averages are located in the rising part of the background curve of $\alpha(CH_3O_2)$ vs. NO. Average values for $\alpha(CH_3O_2)$ were around 0.4 for ATom and close to 0.6 for CAFE Africa and CAFE Brazil, which means that 60 and 40 %, respectively, of the available peroxy radicals reacted with HO_2 and terminated the O_3-forming HO_x cycle. This is expected given low NO mixing ratios in the remote tropical regions or over tropical waters. The OMO data set showed VOC-sensitive O_3 chemistry at the surface with $\alpha(CH_3O_2)$=0.96, indicating that almost all peroxy radicals reacted with NO instead of HO_2. However, as mentioned above, the very limited number of data points available at low altitude for the OMO campaign were all captured in proximity to airports and therefore do not represent surface conditions in the Middle East or over the Indian Ocean. Figure 5 (b) shows the results for the free troposphere between 2 and 10 km altitude. All campaigns showed a clear NO_x-sensitive O_3 chemistry, which again is expected in the absence of NO sources at these altitudes and aligns with the observations from the vertical profiles in Figure 4. In Figure 5 (c), upper tropospheric data (above 10 km) are presented. The upper troposphere over the remote Pacific Ocean was clearly NO_x-sensitive. The remaining areas were located in a transition regime with average values for $\alpha(CH_3O_2)$ of between 0.78 and 0.92 and for NO of between 0.07 and 0.15 ppbv, whereby ATom Atlantic tended towards NO_x sensitivity and the remaining campaigns towards VOC-sensitive O_3 chemistry. The data points additionally show a large 1σ standard deviation in the order of 100 % for NO. This underlines the large variability of NO mixing ratios in the upper troposphere caused by clean NO-free air transported from the boundary layer via

Figure 5. Overview of determination of O_3 sensitivity via (a)-(c) $\alpha(CH_3O_2)$ and (d)-(f) O_3 versus NO mixing ratios separated into the surface below $2\,km$ ((a) and (d)), the free troposphere between 2 and $10\,km$ ((b) and (e)) and the upper troposphere above $10\,km$ ((c) and (f)). Black lines represent the tropical background as an average of all available data points binned to NO, with $1\,\sigma$ standard deviations shown as gray areas. The colored data points and error bars present the campaign averages and $1\,\sigma$ standard deviations, respectively. CAFE Brazil averages are shown in blue, CAFE Africa in red, ATom Pacific in cyan, ATom Atlantic in orange and OMO in green. The gray dotted line in panels (c) and (f) shows the number of data points in each NO bin.

convective processes and strong, local NO emissions from lightning. We identified $< 5\,\%$ and $< 10\,\%$ of data points as being impacted by lightning for ATom Pacific and ATom Atlantic, respectively, demonstrating NO_x-sensitive chemistry. For the remaining campaigns, lightning impacted a much higher share of data points ($\sim 20\,\%$ for CAFE Brazil, $\sim 40\,\%$ for CAFE Africa and $\sim 50\,\%$ for OMO), resulting in higher values for $\alpha(CH_3O_2)$.

These observations are confirmed when looking at O_3 versus NO mixing ratios as displayed in the lower panels (d)-(f) of Figure 5. The black line and gray error shading represent background O_3 binned to NO, including all available data points. For NO_x-sensitive chemistry approximately up to 0.1–0.15 ppbv NO, O_3 increases from 30 to 60 ppbv with increasing NO. Our hypothesis is that in this rising part both peroxy self-reaction and NO to NO_2 oxidation via peroxy radicals play a significant role, the latter path leading to O_3 formation in the presence of sunlight and oxygen. With increasing amounts of NO, O_3 levels rise. In turn, when NO is present in excess over peroxy radicals, O_3 levels reach a maximum, as its formation is limited by the availability of peroxy radicals. At the surface, as shown in Figure 5 (d), O_3 average values for CAFE Brazil, CAFE Africa, ATom Atlantic and ATom Pacific were low, ranging from 20 to 35 ppbv. O_3 for OMO was higher which correlated with higher NO captured from airport emissions. Slightly higher O_3 levels between 35 and 55 ppbv were observed for the free troposphere, which can be seen in Figure 5 (e). These elevated values compared to the surface cannot be explained by photochemical formation in the NO-poor free troposphere, but are likely rather an outcome of transport processes. Upper tropospheric values for O_3 versus NO are presented in Figure 5 (f) and show similar features compared to $\alpha(CH_3O_2)$ in panel (c). Low average O_3 (37 ppbv) and NO (0.04 ppbv) indicate NO_x-sensitive chemistry in the upper troposphere over the remote Pacific Ocean during the ATom campaign. The

Figure 6. Overview of determination of O_3 sensitivity via (a)-(b) $\alpha(CH_3O_2)$ and (c)-(d) O_3 versus NO mixing ratios separated into data with ((b) and (d)) and without impact from lightning ((a) and (c)).

remaining data points were located mostly in the transition area. Maximum average values of O_3 of > 60 ppbv were observed for CAFE Africa, going hand-in-hand with high shares of lightning-impacted data. In contrast, O_3 average values for ATom Atlantic (56 ppbv) were much higher than those observed for OMO (46 ppbv), even though less than 10 % of the data points were impacted by lightning during ATom versus 50 % during OMO. This underlines that while the correlation of O_3 with NO can provide valuable hints for sensitivity investigations, it cannot be solely captured by photochemistry and could also be impacted by transport process from the stratosphere or tropospheric events, e.g., biomass burning, and has a longer upper tropospheric lifetime than NO. The O_3-NO correlation should therefore be used in combination with a reliable metric such as $\alpha(CH_3O_2)$.

3.4 Impact of Lightning

We have investigated the role of lightning in O_3 sensitivity by applying a filter for lightning impact. We categorize data points above 2 km altitude and with NO mixing ratios higher than 0.1 ppbv as impacted by lightning. If the observed NO value is lower, we assume that the data point was not directly impacted by lightning. We expect the contribution of aircraft to the overall NO_x emissions in the tropical troposphere to be insignificant (Grewe, 2007; Nussbaumer et al., 2023). Figure 6 presents the O_3 sensitivity analysis based on $\alpha(CH_3O_2)$ and O_3 vs. NO, following the similar scheme as in Figure 5, separated into data points impacted and not impacted by lightning. The share of data points in each average value depends on the campaign, for example, for ATom Pacific more than 95 % fall into the category without lightning, whereas it is 50 % for OMO. The background curves are the same as those presented in Figure 5.

Figure 6 (a) shows $\alpha(CH_3O_2)$ vs. NO for data points without lightning impact. All five campaign averages were located in the rising part of the background curve with values for $\alpha(CH_3O_2)$ between 0.56 and 0.82, indicating distinct NO_x-sensitive O_3 chemistry. In comparison, Figure 6 (b) presents data points with lightning impact. In all cases, in-

dependent of the latitude, $\alpha(CH_3O_2)$ was high and close to 1. This shows that available peroxy radicals dominantly reacted with NO resulting in the formation of O_3, indicating VOC-sensitive chemistry. The $1\,\sigma$ standard deviations (shown by the error bars) are quite large because lightning induces highly variable amounts of NO and additionally, we do not distinguish between fresh and aged lightning in this view. For CAFE Brazil, for example, we observed peak values of more than $2\,ppbv$ NO (factor 4 compared to the shown scale).

Figure 6 (c) shows O_3 vs. NO for data points not impacted by lightning. O_3 average values ranged between 35 and $55\,ppbv$. In comparison, the average values impacted by lightning were located at much higher O_3 mixing ratios (between 55 and $80\,ppbv$) and in the part of the background where O_3 becomes unresponsive to NO, as shown in panel (d). These results support the findings from $\alpha(CH_3O_2)$ and show that lightning plays an important role in the sensitivity of O_3 formation towards its precursors.

4 Conclusion and Outlook

In this study, we presented in situ measurements of NO, O_3 and HO_2 from four different research aircraft campaigns in the tropical troposphere. These are the OMO campaign in 2015 over the Middle East and the Indian Ocean, the CAFE Africa campaign in 2018 over the Atlantic Ocean, the ATom campaign between 2016 and 2018 around the American continent and the CAFE Brazil campaign in 2022/23 over Brazil. We separated the ATom campaign into a part over the remote Pacific Ocean and a part over the Atlantic Ocean. All data is filtered for the troposphere ($< 100\,ppbv$ O_3) and for tropical latitudes (30°S - 30°N). We compared the in situ measurements with modeled data by the ECHAM5/MESSy2 Atmospheric Chemistry (EMAC) model and found good agreement with a correlation coefficient mostly ranging between 0.5 and 0.8 and standard deviations mostly similar to the respective experimental data set. The largest discrepancies were found for the modeled NO for CAFE Africa. Based on these findings, we used the HO_2 modeled data for CAFE Brazil, as final experimental data were not available. We found low mixing ratios for NO at the surface and in the free troposphere across the remote tropical latitudes, underlining the absence of sources at these altitudes. Mixing ratios in the upper troposphere were elevated compared to the lower altitudes with highest values over tropical continents (compared to tropical waters), and coincided with the location of maximum deep convection and the ITCZ, where lighting activity peaks. HO_2 was mostly similar in the campaign inter-comparison and large variability made it difficult to identify significant differences. O_3 vertical profiles show signs of deep convective processes, especially for the CAFE Brazil campaign. Mixing ratios were lowest over the remote Pacific Ocean and higher for areas impacted by emissions, e.g., biomass burning, such as CAFE Africa.

We investigated O_3 sensitivity using O_3 mixing ratios and the metric $\alpha(CH_3O_2)$ correlated with ambient NO. We found that O_3 chemistry at the surface and the free troposphere was almost exclusively sensitive to NO_x. The only exception was the OMO campaign, where we observed VOC-sensitive O_3 chemistry at the surface due to the capture of anthropogenic pollution from airports. For the upper troposphere, we found NO_x-sensitive O_3 chemistry over the remote Pacific Ocean during ATom and a transition regime for the other campaigns, with the value for $\alpha(CH_3O_2)$ increasing with the amount of lightning observed. Separating data points with and without lightning impact showed that lightning is the most important factor controlling O_3 sensitivity in the tropical troposphere. In the absence of lightning, chemistry was NO_x-sensitive, while it was strongly VOC-sensitive in the presence of lightning, independent of the exact location in the tropical region.

These results are in line with our previous findings in the upper tropical troposphere, which were based entirely on modeling simulations (Nussbaumer et al., 2023). This un-

derlines effectively that $\alpha(\text{CH}_3\text{O}_2)$ is a powerful metric for identifying O_3 sensitivity and it is applicable both to modeled data and in situ observations. It also shows that NO_x is the predominant factor determining O_3 sensitivity and in the tropics its major source is lightning, which in turn depends on the time of year and the distance to tropical landmasses. Photochemical O_3 formation is capped by the availability of peroxy radicals in areas impacted by lightning. From this, we conclude that potential increases in lightning in these regions will likely not impact the amount of O_3, given that levels of peroxy radicals remain unchanged. In turn, increases in lightning in regions that are currently not or only mildly impacted by lightning might lead to increases of O_3 levels up to a factor of 2, which could strongly impact the radiative forcing (especially at high altitudes). The remote tropical lower troposphere currently has only a small number of NO sources. This could change in the future if biomass burning events would become more frequent with increasing temperature and decreasing precipitation and if countries in the Global South increase NO_x emissions associated with the expansion of their economies. Combined with NO_x-sensitive O_3 chemistry, this would lead to strong increases of O_3 levels, which could locally harm plants and human health or, given the lifetime of O_3 of a few weeks, be transported to areas where it has adverse effects.

Looking into the future, further research should investigate the changing role of NO_x in tropospheric O_3 chemistry. While we can say that NO_x is the most important driver of O_3 sensitivity, future changes and North-South re-locations in NO_x emissions, such as expected changes in emissions from anthropogenic combustion processes or increases in biomass burning, will profoundly influence tropospheric photochemistry, and in turn air quality and climate change.

Open Research Section

The dataset for the OMO campaign can be obtained from the HALO database (last access: 23.10.2023) (Deutsches Zentrum für Luft- und Raumfahrt (DLR), 2021). The ATom dataset is available at Wofsy et al. (2021) (last access: 15.09.2023). The datasets for CAFE Africa and CAFE Brazil are not yet published and will be uploaded upon acceptance of the manuscript.

Acknowledgments

References

Ainsworth, E. A., Yendrek, C. R., Sitch, S., Collins, W. J., & Emberson, L. D. (2012). The effects of tropospheric ozone on net primary productivity and implications for climate change. *Annual review of plant biology*, *63*(1), 637–661. doi: 10.1146/annurev-arplant-042110-103829

Akimoto, H., & Tanimoto, H. (2022). Rethinking of the adverse effects of nox-control on the reduction of methane and tropospheric ozone–challenges toward a denitrified society. *Atmospheric Environment*, *277*, 119033. doi: 10.1016/j.atmosenv.2022.119033

Archibald, A. T., Neu, J. L., Elshorbany, Y. F., Cooper, O. R., Young, P. J., Akiyoshi, H., ... Zeng, G. (2020). Tropospheric ozone assessment report: A critical review of changes in the tropospheric ozone burden and budget from 1850 to 2100. *Elementa: Science of the Anthropocene*, *8*(1), 034. doi: 10.1525/elementa.2020.034

Bourgeois, I., Peischl, J., Neuman, J. A., Brown, S. S., Allen, H. M., Campuzano-

Jost, P., ... Ryerson, T. B. (2022). Comparison of airborne measurements of no, no$_2$, hono, no$_y$, and co during firex-aq. *Atmospheric Measurement Techniques*, *15*(16), 4901–4930. doi: 10.5194/amt-15-4901-2022

Bourgeois, I., Peischl, J., Neuman, J. A., Brown, S. S., Thompson, C. R., Aikin, K. C., ... Ryerson, T. B. (2021). Large contribution of biomass burning emissions to ozone throughout the global remote troposphere. *Proceedings of the National Academy of Sciences*, *118*(52), e2109628118. doi: 10.1073/pnas.2109628118

Brasseur, G. P., Müller, J.-F., & Granier, C. (1996). Atmospheric impact of nox emissions by subsonic aircraft: A three-dimensional model study. *Journal of Geophysical Research: Atmospheres*, *101*(D1), 1423–1428. doi: 10.1029/95JD02363

Bray, C. D., Battye, W. H., Aneja, V. P., & Schlesinger, W. H. (2021). Global emissions of nh3, nox, and n2o from biomass burning and the impact of climate change. *Journal of the Air & Waste Management Association*, *71*(1), 102–114. doi: 10.1080/10962247.2020.1842822

Christian, H. J., Blakeslee, R. J., Boccippio, D. J., Boeck, W. L., Buechler, D. E., Driscoll, K. T., ... Stewart, M. F. (2003). Global frequency and distribution of lightning as observed from space by the optical transient detector. *Journal of Geophysical Research: Atmospheres*, *108*(D1), ACL–4. doi: 10.1029/2002JD002347

Cooper, O. R., Parrish, D., Ziemke, J., Balashov, N., Cupeiro, M., Galbally, I., ... Zbinden, R. M. (2014). Global distribution and trends of tropospheric ozone: An observation-based review. *Elementa: Science of the Anthropocene*, *2*. doi: 10.12952/journal.elementa.000029

Crutzen, P. J. (1988). *Tropospheric ozone: An overview.* Springer. doi: 10.1007/978 -94-009-2913-5_1

Deutsches Zentrum für Luft- und Raumfahrt (DLR). (2021). *Mission:OMO.* (https://halo-db.pa.op.dlr.de/mission/0, last access on 23.10.2023)

Faloona, I. C., Tan, D., Lesher, R. L., Hazen, N. L., Frame, C. L., Simpas, J. B., ... Brune, W. H. (2004). A laser-induced fluorescence instrument for detecting tropospheric oh and ho 2: Characteristics and calibration. *Journal of Atmospheric Chemistry*, *47*, 139–167. doi: 10.1023/B:JOCH.0000021036.53185.0e

Gaudel, A., Bourgeois, I., Li, M., Chang, K.-L., Ziemke, J., Sauvage, B., ... Cooper, O. R. (2024). Tropical tropospheric ozone distribution and trends from in situ and satellite data. *EGUsphere*, *2024*, 1–51.

Gough, W. A., & Anderson, V. (2022). Changing air quality and the ozone weekend effect during the covid-19 pandemic in toronto, ontario, canada. *Climate*, *10*(3), 41. doi: 10.3390/cli10030041

Granier, C., Darras, S., Denier van der Gon, H., Doubalova, J., Elguindi, N., Galle, B., ... Sindelarova, K. (2019). The copernicus atmosphere monitoring service global and regional emissions (april 2019 version). *Copernicus Atmosphere Monitoring Service (CAMS) report*. doi: 10.24380/d0bn-kx16

Grewe, V. (2007). Impact of climate variability on tropospheric ozone. *Science of the total environment*, *374*(1), 167–181. doi: 10.1016/j.scitotenv.2007.01.032

Grewe, V., Brunner, D., Dameris, M., Grenfell, J., Hein, R., Shindell, D., & Staehelin, J. (2001). Origin and variability of upper tropospheric nitrogen oxides and ozone at northern mid-latitudes. *Atmospheric Environment*, *35*(20), 3421-3433. doi: 10.1016/S1352-2310(01)00134-0

Hamryszczak, Z., Dienhart, D., Brendel, B., Rohloff, R., Marno, D., Martinez, M., ... others (2023). Measurement report: Hydrogen peroxide in the upper tropical troposphere over the atlantic ocean and western africa during the cafe-africa aircraft campaign. *Atmospheric Chemistry and Physics*, *23*(10), 5929–5943. doi: 10.5194/acp-23-5929-2023

Hersbach, H., Bell, B., Berrisford, P., Hirahara, S., Horányi, A., Muñoz-Sabater, J.,

... Thépaut, J.-N. (2020). The era5 global reanalysis. *Quarterly Journal of the Royal Meteorological Society*, *146*(730), 1999-2049. doi: 10.1002/qj.3803

Iglesias-Suarez, F., Kinnison, D. E., Rap, A., Maycock, A. C., Wild, O., & Young, P. J. (2018). Key drivers of ozone change and its radiative forcing over the 21st century. *Atmospheric Chemistry and Physics*, *18*(9), 6121–6139. doi: 10.5194/acp-18-6121-2018

IPCC. (2023). Sections. in: Climate change 2023: Synthesis report. contribution of working groups i, ii and iii to the sixth assessment report of the intergovernmental panel on climate change [core writing team, h. lee and j. romero (eds.)]. , 35–115. doi: 10.59327/IPCC/AR6-9789291691647

Jaeglé, L., Jacob, D. J., Brune, W., Faloona, I., Tan, D., Kondo, Y., ... others (1999). Ozone production in the upper troposphere and the influence of aircraft during sonex: Approach of nox-saturated conditions. *Geophysical Research Letters*, *26*(20), 3081–3084. doi: 10.1029/1999GL900451

Jaeglé, L., Jacob, D. J., Brune, W., Tan, D., Faloona, I., Weinheimer, A., ... Sachse, G. (1998). Sources of hox and production of ozone in the upper troposphere over the united states. *Geophysical Research Letters*, *25*(10), 1709–1712. doi: 10.1029/98GL00041

Jaffe, D. A., Ninneman, M., & Chan, H. C. (2022). Nox and o3 trends at us non-attainment areas for 1995–2020: Influence of covid-19 reductions and wildland fires on policy-relevant concentrations. *Journal of Geophysical Research: Atmospheres*, *127*(11), e2021JD036385. doi: 10.1029/2021JD036385

Jöckel, P., Tost, H., Pozzer, A., Kunze, M., Kirner, O., Brenninkmeijer, C. A., ... Zahn, A. (2016). Earth system chemistry integrated modelling (escimo) with the modular earth submodel system (messy) version 2.51. *Geoscientific Model Development*, *9*(3), 1153–1200. doi: 10.5194/gmd-9-1153-2016

Künstler, C. (2020). *Measurements of atmospheric oh and ho2 radicals by laser-induced fluorescence on the halo aircraft during the omo-asia 2015 campaign* (Doctoral dissertation, Universität zu Köln). Retrieved from `http://kups.ub.uni-koeln.de/id/eprint/11702`

Lacis, A. A., Wuebbles, D. J., & Logan, J. A. (1990). Radiative forcing of climate by changes in the vertical distribution of ozone. *Journal of Geophysical Research: Atmospheres*, *95*(D7), 9971–9981. doi: 10.1029/JD095iD07p09971

Lelieveld, J., Bourtsoukidis, E., Brühl, C., Fischer, H., Fuchs, H., Harder, H., ... Ziereis, H. (2018). The south asian monsoon—pollution pump and purifier. *Science*, *361*(6399), 270–273. doi: 10.1126/science.aar2501

Lelieveld, J., & Dentener, F. J. (2000). What controls tropospheric ozone? *Journal of Geophysical Research: Atmospheres*, *105*(D3), 3531–3551. doi: 10.1029/1999JD901011

Lelieveld, J., Gromov, S., Pozzer, A., & Taraborrelli, D. (2016). Global tropospheric hydroxyl distribution, budget and reactivity. *Atmospheric Chemistry and Physics*, *16*(19), 12477–12493. doi: 10.5194/acp-16-12477-2016

Li, K., Jacob, D. J., Liao, H., Shen, L., Zhang, Q., & Bates, K. H. (2019). Anthropogenic drivers of 2013–2017 trends in summer surface ozone in china. *Proceedings of the National Academy of Sciences*, *116*(2), 422–427. doi: 10.1073/pnas.1812168116

Liu, C., & Shi, K. (2021). A review on methodology in o3-nox-voc sensitivity study. *Environmental Pollution*, *291*, 118249. doi: 10.1016/j.envpol.2021.118249

Marno, D., Ernest, C., Hens, K., Javed, U., Klimach, T., Martinez, M., ... Harder, H. (2020). Calibration of an airborne ho x instrument using the all pressure altitude-based calibrator for ho x experimentation (apache). *Atmospheric measurement techniques*, *13*(5), 2711–2731. doi: 10.5194/amt-13-2711-2020

McDonald, B. C., De Gouw, J. A., Gilman, J. B., Jathar, S. H., Akherati, A., Cappa, C. D., ... Trainer, M. (2018). Volatile chemical products emerging as largest petrochemical source of urban organic emissions. *Science*, *359*(6377),

760–764. doi: 10.1126/science.aaq0524

McDuffie, E. E., Smith, S. J., O'Rourke, P., Tibrewal, K., Venkataraman, C., Marais, E. A., . . . Martin, R. V. (2020). A global anthropogenic emission inventory of atmospheric pollutants from sector- and fuel-specific sources (1970–2017): an application of the community emissions data system (ceds). *Earth System Science Data*, *12*(4), 3413–3442. doi: 10.5194/essd-12-3413-2020

NASA. (2022). *Atom.* Retrieved from `"https://espo.nasa.gov/atom"` (accessed on 2023-11-15)

Novelli, A., Hens, K., Tatum Ernest, C., Kubistin, D., Regelin, E., Elste, T., . . . Harder, H. (2014). Characterisation of an inlet pre-injector laser-induced fluorescence instrument for the measurement of atmospheric hydroxyl radicals. *Atmospheric measurement techniques*, *7*(10), 3413–3430. doi: 10.5194/amt-7-3413-2014

Nussbaumer, C. M. (2023). *Nitrogen oxides and their involvement in photochemical processes throughout the troposphere* (Doctoral dissertation, Universität Mainz). doi: 10.25358/openscience-9272

Nussbaumer, C. M., & Cohen, R. C. (2020). The role of temperature and no$_x$ in ozone trends in the los angeles basin. *Environmental Science & Technology*, *54*, 15652–15659. doi: 10.1021/acs.est.0c04910

Nussbaumer, C. M., Crowley, J. N., Schuladen, J., Williams, J., Hafermann, S., Reiffs, A., . . . Fischer, H. (2021). Measurement report: Photochemical production and loss rates of formaldehyde and ozone across europe. *Atmospheric Chemistry and Physics*, *21*(24), 18413–18432. doi: 10.5194/acp-21-18413-2021

Nussbaumer, C. M., Fischer, H., Lelieveld, J., & Pozzer, A. (2023). What controls ozone sensitivity in the upper tropical troposphere? *Atmospheric Chemistry and Physics*, *23*(19), 12651–12669. doi: 10.5194/acp-23-12651-2023

Nussbaumer, C. M., Parchatka, U., Tadic, I., Bohn, B., Marno, D., Martinez, M., . . . J. Lelieveld, H. F. (2021). Modification of a conventional photolytic converter for improving aircraft measurements of no$_2$ via chemiluminescence. *Atmospheric measurement techniques*, *14*(10), 6759–6776. doi: 10.5194/amt-14-6759-2021

Nussbaumer, C. M., Pozzer, A., Tadic, I., Röder, L., Obersteiner, F., Harder, H., . . . Fischer, H. (2022). Tropospheric ozone production and chemical regime analysis during the covid-19 lockdown over europe. *Atmospheric Chemistry and Physics*, *22*(9), 6151–6165. doi: 10.5194/acp-22-6151-2022

Nussbaumer, C. M., Tadic, I., Dienhart, D., Wang, N., Edtbauer, A., Ernle, L., . . . Fischer, H. (2021). Measurement report: In situ observations of deep convection without lightning during the tropical cyclone florence 2018. *Atmospheric Chemistry and Physics*, *21*(10), 7933–7945. doi: 10.5194/acp-21-7933-2021

Nuvolone, D., Petri, D., & Voller, F. (2018). The effects of ozone on human health. *Environmental Science and Pollution Research*, *25*(9), 8074–8088. doi: 10.1007/s11356-017-9239-3

Obersteiner, F. (2023). *Fairo.* Retrieved from `https://gitlab.kit.edu/FObersteiner/FAIROmeta/-/blob/main/science/FAIRO_Description.md` (accessed on 2024-03-07)

Pope, R. J., Arnold, S. R., Chipperfield, M. P., Reddington, C. L., Butt, E. W., Keslake, T. D., . . . others (2020). Substantial increases in eastern amazon and cerrado biomass burning-sourced tropospheric ozone. *Geophysical Research Letters*, *47*(3), e2019GL084143. doi: 10.1029/2019GL084143

Pusede, S. E., Steiner, A. L., & Cohen, R. C. (2015). Temperature and recent trends in the chemistry of continental surface ozone. *Chemical reviews*, *115*(10), 3898–3918. doi: 10.1021/cr5006815

Roeckner, E., Brokopf, R., Esch, M., Giorgetta, M., Hagemann, S., Kornblueh, L., . . . Schulzweida, U. (2006). Sensitivity of simulated climate to horizontal

and vertical resolution in the echam5 atmosphere model. *Journal of Climate*, *19*(16), 3771–3791.

Schumann, U., & Huntrieser, H. (2007). The global lightning-induced nitrogen oxides source. *Atmospheric Chemistry and Physics*, *7*(14), 3823–3907. doi: 10.5194/acp-7-3823-2007

Sicard, P., Paoletti, E., Agathokleous, E., Araminienė, V., Proietti, C., Coulibaly, F., & De Marco, A. (2020). Ozone weekend effect in cities: Deep insights for urban air pollution control. *Environmental Research*, *191*, 110193. doi: 10.1016/j.envres.2020.110193

Sillman, S. (1995). The use of NO_y, H_2O_2, and HNO_3 as indicators for ozone-NO_x-hydrocarbon sensitivity in urban locations. *Journal of Geophysical Research: Atmospheres*, *100*(D7), 14175–14188. doi: 10.1029/94JD02953

Skeie, R. B., Myhre, G., Hodnebrog, Ø., Cameron-Smith, P. J., Deushi, M., Hegglin, M. I., . . . Wu, T. (2020). Historical total ozone radiative forcing derived from cmip6 simulations. *Npj Climate and Atmospheric Science*, *3*(1), 32. doi: 10.1038/s41612-020-00131-0

Staehelin, J., Harris, N. R., Appenzeller, C., & Eberhard, J. (2001). Ozone trends: A review. *Reviews of Geophysics*, *39*(2), 231–290. doi: 10.1029/1999RG000059

Stratmann, G., Ziereis, H., Stock, P., Brenninkmeijer, C., Zahn, A., Rauthe-Schöch, A., . . . Volz-Thomas, A. (2016). No and noy in the upper troposphere: Nine years of caribic measurements onboard a passenger aircraft. *Atmospheric Environment*, *133*, 93-111. doi: https://doi.org/10.1016/j.atmosenv.2016.02.035

Tadic, I., Crowley, J. N., Dienhart, D., Eger, P., Harder, H., Hottmann, B., . . . Fischer, H. (2020). Net ozone production and its relationship to nitrogen oxides and volatile organic compounds in the marine boundary layer around the arabian peninsula. *Atmospheric Chemistry and Physics*, *20*(11), 6769–6787. doi: 10.5194/acp-20-6769-2020

Tadic, I., Nussbaumer, C., Bohn, B., Harder, H., Marno, D., Martinez, M., . . . Fischer, H. (2021). Central role of nitric oxide in ozone production in the upper tropical troposphere over the atlantic ocean and west africa. *Atmospheric Chemistry and Physics*, *21*(10), 8195–8211. doi: 10.5194/acp-2021-52

Taylor, K. E. (2001). Summarizing multiple aspects of model performance in a single diagram. *Journal of geophysical research: atmospheres*, *106*(D7), 7183–7192. doi: 10.1029/2000JD900719

Thompson, C. R., Wofsy, S. C., Prather, M. J., Newman, P. A., Hanisco, T. F., Ryerson, T. B., . . . Zeng, L. (2022). The nasa atmospheric tomography (atom) mission: Imaging the chemistry of the global atmosphere. *Bulletin of the American Meteorological Society*, *103*(3), E761–E790. doi: 10.1175/BAMS-D-20-0315.1

Tomsche, L., Pozzer, A., Ojha, N., Parchatka, U., Lelieveld, J., & Fischer, H. (2019). Upper tropospheric ch4 and co affected by the south asian summer monsoon during the oxidation mechanism observations mission. *Atmospheric Chemistry and Physics*, *19*(3), 1915–1939. doi: 10.5194/acp-19-1915-2019

Verma, S., Yadava, P. K., Lal, D., Mall, R., Kumar, H., & Payra, S. (2021). Role of lightning nox in ozone formation: A review. *Pure and Applied Geophysics*, *178*, 1425–1443. doi: 10.1007/s00024-021-02710-5

Wennberg, P., Hanisco, T., Jaegle, L., Jacob, D., Hintsa, E., Lanzendorf, E., . . . others (1998). Hydrogen radicals, nitrogen radicals, and the production of o3 in the upper troposphere. *science*, *279*(5347), 49–53. doi: 10.1126/science.279.5347.49

Wofsy, S., Afshar, S., Allen, H., Apel, E., Asher, E., Barletta, B., . . . Vieznor, N. (2021). *Atom: Merged atmospheric chemistry, trace gases, and aerosols, version 2.* ORNL Distributed Active Archive Center. Retrieved from https://daac.ornl.gov/cgi-bin/dsviewer.pl?ds_id=1925 doi:

10.3334/ORNLDAAC/1925

Yan, Y. Y. (2005). Intertropical convergence zone (itcz). In *Encyclopedia of world climatology* (pp. 429–432). Dordrecht: Springer Netherlands. doi: 10.1007/1 -4020-3266-8_110

Zahn, A., Weppner, J., Widmann, H., Schlote-Holubek, K., Burger, B., Kühner, T., & Franke, H. (2012). A fast and precise chemiluminescence ozone detector for eddy flux and airborne application. *Atmospheric Measurement Techniques*, *5*(2), 363–375. doi: 10.5194/amt-5-363-2012

Zhao, Y., Li, Y., Kumar, A., Ying, Q., Vandenberghe, F., & Kleeman, M. J. (2022). Separately resolving nox and voc contributions to ozone formation. *Atmospheric Environment*, *285*, 119224. doi: 10.1016/j.atmosenv.2022.119224

Ziereis, H., Schlager, H., Schulte, P., Van Velthoven, P., & Slemr, F. (2000). Distributions of no, no$_x$, and no$_y$ in the upper troposphere and lower stratosphere between 28 and 61 n during polinat 2. *Journal of Geophysical Research: Atmospheres*, *105*(D3), 3653–3664. doi: 10.1029/1999JD90087